Homer, M. E., Champneys, A. R., Hunt, G. W., & Cooper, N. (2003). Mathematical modeling of the radial profile of basilar membrane vibrations in the inner ear. 10.1121/1.1771571

Mathematical modeling of the radial profile of basilar membrane vibrations in the inner ear

Martin Homer[a)]

Alan Champneys

Department of Engineering Mathematics,

University of Bristol,

Bristol BS7 8EX,

United Kingdom

Giles Hunt

Department of Mechanical Engineering,

University of Bath,

Bath BA2 7AY,

United Kingdom

Nigel Cooper

The MacKay Institute of Communication and Neuroscience,

Keele University,

Keele ST5 5BG,

United Kingdom

Abbreviated title: Mathematical modeling of basilar membrane vibrations

22 August 2003

[a)]Electronic mail: martin.homer@bristol.ac.uk

Abstract

Motivated by recent experimental results we seek an explanation of asymmetry in the radial profile of basilar membrane vibrations in the inner ear. We study a sequence of one-dimensional beam models which take into account variations in the bending stiffness of the basilar membrane as well as the potential presence of structural hinges. Our results suggest that the main cause of asymmetry is likely to be differences between the boundary conditions at the two extremes of the basilar membrane's width. This has fundamental implications for more detailed numerical simulations of the entire cochlea.

PACS numbers: **43.64.Kc**, 43.40.At, 43.40.Cw

I. INTRODUCTION

In this report we consider a succession of simple mathematical models which are intended to describe the distribution of sound-evoked vibrations across the width of the inner-ear's basilar membrane. This distribution, which we will refer to as a 'radial profile', has been the subject of several recent experimental studies (e.g. Cooper, 1999; Nilsen and Russell, 1999, 2000; Rhode and Recio, 2000) and has fundamental implications for detailed numerical simulations of the entire cochlea (cf. Steele, 1974; Brass, 2000; Lim, 2000; Barker, 2000).

Figure 1 shows a schematic cross section through the cochlear partition. The basilar membrane (BM, at the bottom of the figure) is thought to be responsible for converting sound-evoked pressure differences between the two sides of the partition (SM and ST in Fig. 1) into 'transverse' structural motion (vertical arrows in Fig. 1). The various support cells and accessory structures which ride on top of the BM convert the transverse motion into shearing motion in the sub-tectorial space (see horizontal arrows in Fig. 1), as is needed to excite the partition's mechano-sensitive inner and outer hair cells (IHC/OHCs) and give rise to the sensation of hearing (Dallos *et al.*, 1996, for reviews). The situation in the real cochlea may be far more complex than this, as has been suggested in various experimental investigations (e.g. Karavitaki *et al.*, 1998; Nilsen and Russell, 1999, 2000). On the other hand, it may not be, as suggested in other investigations (e.g. Richter and Dallos, 1999; Fridberger *et al.*, 2002). Unfortunately, the basic physical characteristics of the components of the cochlea, and the mechanics of their interactions, are not well understood. The only well-established facts are that the BM varies in stiffness between the arcuate and pectinate zones (Miller, 1985; Olson and Mountain, 1994), and that the hair cells and most of the support cells are at least an order of magnitude less stiff than the BM (Hallworth, 1995). The only structures which seem to have a pronounced effect on the local stiffness of the BM are the pillar cells (labelled PC in Fig. 1; cf. Olson and Mountain, 1994; Tolomeo and Holley, 1997). The purpose of the present paper is to investigate the consequences of this structural knowledge in

terms of the mechanical processing of sound in the cochlea.

The experimental studies of the BM's radial profile which have been performed to date have had mixed results: Nilsen and Russell, 1999, 2000 have reported relatively complex radial profiles, while Cooper, 1999 and Rhode and Recio, 2000 have reported much simpler profiles. The present report will focus on the simpler profiles. There are several reasons for this: firstly, the more complex findings of Russell and Nilsen have not been confirmed in independent investigations, while the simpler profiles have been observed by at least two groups. Secondly, the observations made by Cooper, 1999, 2000 are the most extensive available; they map the BM's radial profile with unprecedented resolution and they apply across a wide range of stimulus frequencies, a wide range of intensities at the BM's characteristic frequency, and a number of longitudinal locations in guinea-pig, gerbil and chinchilla cochleae. Cooper's measurements are also consistent with previous radial profile studies in the cat (e.g. Wilson and Evans, 1983; Cooper and Rhode, 1992), despite the differences in physical parameters (such as BM thickness) between species. From the point of view of our mathematical analyses, the most important features of the simple radial profiles are that, at least to a first approximation, the BM moves in phase across its entire width, and the amplitude distribution is asymmetric about the BM's mid-point (cf. Fig. 2).

II. SIMPLE BEAM MODEL

Initially, we shall investigate whether a simple beam equation can provide a suitable model to describe the BM's radial profile. Our main aims are to consider what the appropriate boundary conditions might be, and to consider how variations in the stiffness of the arcuate and pectinate zones might affect the BM's radial profile. Throughout we shall consider only one-dimensional spatial variation of the BM, that is we assume the profile to be a function of radial position only (and not time). We justify this by the experimental observation that the BM vibrates in what appears, within experimental accuracy, to be its pure fundamental

mode, across a wide range of frequencies, intensities, and longitudinal locations along the cochlear partition. Hence we can take a simple, second order in time, sinusoidally forced beam model, expand as a Fourier series and keep only the term in the fundamental frequency. We discard nonlinear terms, as the displacement of the BM is extremely small, being less than 1% of the BM's width. Furthermore, over almost the entire range of measurement, the radial profile of the BM has the same shape, with a pronounced asymmetry .

We are left with a simple model of a one dimensional beam, subject to a constant load representing the amplitude of forcing, whose static solutions describe the mode shape of the BM's vibration.

Initially, let us suppose that the beam has a constant bending stiffness EI (where E is the elastic modulus, with units Nm^{-2}, and I is the area moment of inertia, with units m^4), and is subject to a constant line pressure load q, with units Nm^{-1}. Then the equation governing the transverse displacement w as a function of position along the beam x, both with units m, is the Euler-Bernoulli beam equation

$$\frac{\mathrm{d}^4 w}{\mathrm{d}x^4} = \frac{q}{EI} \tag{1}$$

Therefore

$$w(x) = \frac{q}{4!EI}x^4 + Dx^3 + Cx^2 + Bx + A \tag{2}$$

where A, B, C and D are constants determined from the boundary conditions. It is questionable which boundary conditions most accurately model the physiology. Therefore we shall consider the four possible combinations of clamped ($w = w' = 0$) and simply supported ($w = w'' = 0$) boundary conditions at the two ends of the beam. Throughout this report we non-dimensionalise all lengths by the width of the beam, so that $x = 0$ corresponds to the left hand end of the arcuate zone and $x = 1$ to the right hand end of the pectinate zone in the representation of the BM in figure 1, and the parameter q/EI is non-dimensional.

The values of the constants given by the four combinations of boundary conditions are reported in table I.

Figure 2 shows graphs of the solutions of Eq. (2), together with the experimental results we use throughout this study. Throughout this report we have normalised the deflection w, and the experimental data with which we compare our predictions, such that $\int w(x)\,dx = 1$. The experimental results represent the means and standard deviations of 15 measurements made at various frequencies and intensities in a single guinea-pig cochlea (see Cooper, 1999 for details). Inspection of Fig. 2 shows that the uniform bending stiffness beam model with a simply supported boundary condition at $x = 0$ and a clamped boundary at $x = 1$ (as shown in Fig. 2c) provides the best agreement with experimental data. The closeness of this agreement between theoretical and experimental data motivates the beam equation as a suitable candidate to modify, in order to try and improve the fit.

III. NON-UNIFORM BENDING STIFFNESS

Experimental measurements suggest that the bending stiffness of the BM varies across the width of the membrane. The nature of the variation is somewhat controversial: on the one hand Miller, 1985 has shown that the bending stiffness of the arcuate zone is, on average, around 5 times higher than that of the pectinate zone. On the other hand, however, Olson and Mountain, 1994 have shown that the pectinate zone is around three times more stiff than the arcuate zone. In an attempt to refine our model, then, we shall now allow the bending stiffness (i.e. EI) of the model beam to vary across its width. The variations will first be allowed in a piecewise constant fashion. Our aim is not to derive a novel beam model, as achieved in earlier work (e.g. Allaire *et al.*, 1974, Miller, 1985), but rather to ask which simple modeling hypotheses are consistent with experimental data. As before, we shall consider the four combinations of clamped and simply supported boundary conditions at the endpoints.

We initially choose a piecewise constant bending stiffness given by

$$EI(x) = \begin{cases} EI_1 & x \in [0, x_t) \\ EI_2 & x \in (x_t, 1] \end{cases} \tag{3}$$

where EI_1 and EI_2 are the constant bending stiffnesses of the arcuate and pectinate zones (the regions $[0, x_t)$ and $(x_t, 1]$ respectively). Experimental measurements by Cooper, 1999 suggest a value $x_t = 0.28$ though this value may vary slightly according to position along the cochlear partition, and so we shall also investigate the effect of varying x_t. For simplicity, we also define a stiffness ratio factor, Γ,

$$\Gamma = \frac{EI_2}{EI_1} \tag{4}$$

As the bending stiffness is constant in each region, we may solve the beam equation Eq. (1) in each region to give

$$w(x) = \begin{cases} \frac{q}{4!EI_1}x^4 + D_1x^3 + C_1x^2 + B_1x + A_1 & x \in [0, x_t) \\ \frac{q}{4!EI_2}x^4 + D_2x^3 + C_2x^2 + B_2x + A_2 & x \in (x_t, 1] \end{cases} \tag{5}$$

Now to determine the eight constants of integration $A_{1,2}$, $B_{1,2}$, $C_{1,2}$, and $D_{1,2}$, we must pose boundary conditions at $x = 0$, $x = 1$, and $x = x_t$. The conditions at $x = 0$ and $x = 1$ (clamped or simply supported, for example) give four equations for the integration constants, as before, while those at $x = x_t$, the interface between the two zones, must provide another four equations. In the first instance we choose total continuity, that is continuity of w, w', w'' and w''', at $x = x_t$. The values of the eight constants, for the four possible combinations of these boundary conditions are given in appendix A (note that each value is a function of x_t, Γ, q and EI_2).

Figure 3 shows plots of beam displacement, with the four possible combinations of end boundary conditions, for various values of Γ.

Figure 3 clearly shows two plausible matches between the theoretical prediction of the piecewise constant beam model and the experimental data: clamped/clamped boundary conditions (Fig. 3a), with large Γ, and (arguably rather better) simply supported/clamped end conditions (Fig. 3c), with large or moderate Γ. Both of these models fit the data better than the simple constant stiffness beam model, in that they approximate the peak amplitude, and the decay near $x = 1$, more accurately than the simplest model. In either case, we may reasonably hypothesise that the pectinate zone of the basilar membrane is much stiffer than the arcuate zone, as in the measurements of Olson and Mountain, 1994.

Figure 4 shows the effect of varying x_t for fixed Γ. We choose to vary x_t between 0.2 and 0.4; this could represent uncertainty in the position of the interface, or a variation with location in the cochlea. We fix $\Gamma = 25$, as this provided the most plausible match between theoretical prediction and experimental data above.

Figure 4 shows that varying the interface position has a negligible effect on the shape of the model predictions. It seems that the boundary conditions have a far more important effect in governing the mode shape than the position of the junction between the arcuate and pectinate zones. This conclusion is supported by analyses at other values of Γ, including the limit $\Gamma \to \infty$.

IV. RIGID ROD AND HINGE MODEL

With reference to the physiology of the BM, it seems possible that the presence of the pillar cells might make an extremely rigid structure in the arcuate zone, while the joint between the arcuate and pectinate zones of the BM may be relatively weak. The conditions of total continuity proposed thus far may therefore be too strong. This prompts us to consider another simplified model for the basilar membrane, in which the arcuate zone is modelled

by a rigid rod, and the pectinate zone as a flexible beam of constant bending stiffness EI. Thus the equations for the deflection $w(x)$ are

$$w(x) = \begin{cases} B_1 x & x \in [0, x_t) \\ \dfrac{q}{4!EI}x^4 + D_2 x^3 + C_2 x^2 + B_2 x + A_2 & x \in (x_t, 1] \end{cases} \tag{6}$$

We suppose that there is a hinge, or rotational spring, at $x = 0$, such that the slope of the BM there is proportional to the load applied q, so

$$B_1 = \frac{\kappa q}{EI} \tag{7}$$

where the factor EI is inserted to simplify the calculation. Note that small κ represents a relatively stiffer hinge. We now need four boundary conditions for the four unknowns A_2, B_2, C_2, D_2. As before, we allow the beam to be simply supported or clamped at $x = 1$ so that, at $x = 1$

$$w = 0, \quad \text{and either } \frac{\mathrm{d}w}{\mathrm{d}x} = 0 \text{ or } \frac{\mathrm{d}^2 w}{\mathrm{d}x^2} = 0 \tag{8}$$

At the junction $x = x_t$, we suppose either that the beam and rod are "clamped" so that

$$w(x) \text{ and } \frac{\mathrm{d}w}{\mathrm{d}x} \text{ are continuous} \tag{9}$$

at $x = x_t$, or "simply supported", so that

$$w(x) \text{ and } \frac{\mathrm{d}^2 w}{\mathrm{d}x^2} = 0 \text{ are continuous} \tag{10}$$

at $x = x_t$.

Equations (8) together with either Eq. (9) or Eq. (10) give us 4 conditions for the 4 unknowns. As before, these conditions may be solved explicitly to find the four constants of integration

A_2, B_2, C_2, D_2, (as functions of x, x_t and κ) and hence give an analytic expression for the membrane displacement. The values of the constants are reported in appendix B.

Figure 5 shows solutions of Eq. (6) for the four possible combinations of boundary conditions given in Eq. (8) and either Eq. (9) or Eq. (10). The most plausible match to the data in this case is where the membrane is pinned at $x = x_t$ and clamped at $x = 1$ for $\kappa \approx 0.02$, as shown in Fig. 5(c). Varying x_t was again found not to have any significant effect, as shown for the case of two bending stiffness models above. Once again we see the importance of the boundary conditions.

V. CONTINUOUSLY VARIABLE BENDING STIFFNESS

Another possible refinement of our model is to allow the bending stiffness of the BM to vary continuously with position. While the arcuate zone of the real BM has a reasonably constant cross-sectional area and composition, and is therefore quite likely to have a constant bending stiffness, the pectinate zone certainly does not (cf. Iurato, 1962; Cabezudo, 1978). The individual fibrils of collagen which make up the BM are often arranged in such a way that the BM's pectinate zone has two distinct layers (cf. Fig. 6). The layers are separated by a ground substance with potential load-carrying ability, and the thickness of this ground substance varies across the width of the pectinate zone (Iurato, 1962; Cabezudo, 1978); the variation is particularly marked in the unfixed gerbil cochlea, as shown by Edge *et al.*, 1998. In mechanical terms, the resultant variation in the cross sectional area of the pectinate zone will lead to a non constant second moment of area, $I = I(x)$. In this case, we must solve a generalised beam equation:

$$\frac{\mathrm{d}^2}{\mathrm{d}x^2}\left(EI(x)\frac{\mathrm{d}^2 w}{\mathrm{d}x^2}\right) = q \tag{11}$$

We suppose that the BM has uniform cross section along the plane of the membrane; the approximation to the transverse geometry of the cross section used in this study is shown in Fig. 6. We assume that the distance from the centre line (the x-axis) to each edge of the

BM in the arcuate zone is a constant, r. In the pectinate zone, we assume that the BM is divided in two, each half having constant thickness r, and that the profile of the inner and outer edges is quadratic and symmetric about the x-axis and the midpoint of the pectinate zone, $x = (1 + x_t)/2$, with maximum distance from the centre line to the outer edge of the membrane R; thus the distances of the inner and outer edges from the centre line, for $x \in [x_t, 1]$, are given by

$$r_{inner}(x) = \frac{4}{(1-x_t)^2}(R-r)(x-x_t)(1-x) \tag{12}$$

$$r_{outer}(x) = \frac{4}{(1-x_t)^2}(R-r)(x-x_t)(1-x) + r \tag{13}$$

In reality, the upper and lower portions of the pectinate zone of the BM are tied together, both by exchange of fibres between the two portions, and via a ground substance. We shall suppose, for simplicity, that the two portions are joined by a light net of fibres with infinite shear stiffness, and so act together as a competent beam.

Since all lengths are non-dimensionalised by the width of the beam, the second moment of area of a thin slice of membrane is given by Gere and Timoshenko, 1991

$$I(x) = \begin{cases} \frac{2}{3}r^3 & x \in [0, x_t) \\ \frac{2}{3}\left(r_{outer}(x)^3 - r_{inner}(x)^3\right) & x \in (x_t, 1] \end{cases} \tag{14}$$

Direct measurement in the guinea-pig by Miller, 1985 suggests values for the dimensional physical constants r and R of

$$r = 0.75\mu\text{m}; \quad R = 2.15\mu\text{m} \tag{15}$$

for a membrane of width 150μm, so in our non-dimensionalised variables we have that

$$r = \frac{1}{200}; \quad R = \frac{43}{3000} \tag{16}$$

Figure 6 shows a plot of the variation of second moment of area in this case: the average bending stiffness of the pectinate zone is clearly much larger than that in the arcuate zone.

Once again, in order to solve Eq. (11), we must supply end boundary and junction conditions. We shall assume that the modulus of elasticity E is constant and equal in both zones. Figure 7 shows plots of the solution of Eq. (11) together with experimental data for the four possible combinations of clamped or simply supported boundary conditions at the two ends ($x = 0$ and $x = 1$) with total continuity at the junction. Given the values of the constants r and R and the boundary conditions, Eq. (11) can be integrated using Waterloo Maple Software, 1996 to give explicit solutions, shown in Fig. 7. Once again we see reasonable agreement between theory and experiment, best of all when the beam is simply supported at $x = 0$ and clamped at $x = 1$ (cf. Fig. 7c). However, the fit between experiment and data is not as close as that for the piecewise constant bending stiffness model of Figs. 3a and 3c. It appears that the boundary conditions are much more important than the fine details of the model in determining the fundamental behaviour of the membrane.

VI. CONCLUSIONS AND FURTHER WORK

In this report we have discussed simple beam equations as possible models to describe the radial profile of the basilar membrane's sound-evoked vibrations. Part of the benefit of using such simple models is that closed form solutions can be obtained, and so complete parametric studies can be made; a task that is much more difficult with finite element solution methods, for example.

It seems that solutions of the beam equation can fit experimental data well with certain combinations of boundary conditions and bending stiffness variations. The best fit to experimental data is obtained for a beam with piecewise constant bending stiffness, simply supported at the arcuate end ($x = 0$), and clamped at the pectinate end ($x = 1$), with the bending stiffness of the pectinate zone much larger than that of the arcuate zone. Good

agreement is also obtained in the limit of this ratio of bending stiffnesses tending to infinity, with the membrane clamped at the pectinate end, and either simply supported or clamped at the arcuate end. More detailed modelling of the physiology, such as changing the location of the transition from arcuate to pectinate zone, or allowing the bending stiffness of the pectinate zone to vary with radial position, do not substantially improve the fit to experimental data. The more detailed models do support the conclusion, however, that the pectinate zone of the BM is substantially stiffer than the arcuate zone, and that the membrane is simply supported at the arcuate end and clamped at the pectinate end.

We may tentatively conclude, therefore, that the basilar membrane acts as if it is simply supported at the arcuate end, clamped at the pectinate end, and is substantially stiffer in the pectinate zone than the arcuate zone.

There are many possibilities for refinements and improvements to the types of model discussed here. Although a more detailed modelling of the physiology would perhaps be possible, not too much should be expected from a constant loading model; the fit is already reasonably good, given the large standard deviation in the data. Also, we have made no attempt to model the variation of BM properties with position in the cochlear partition, although experimental data suggests that such variation does not significantly affect the qualitative features of the radial profile. Perhaps more important would be to add a simple model of the dynamics of the hair cells, which seem to be largely responsible for enhancing the sensitivity of the BM at low stimulus levels, and try to understand their behaviour in active and passive modes.

APPENDIX A. CONSTANTS OF INTEGRATION FOR THE PIECEWISE CONSTANT BENDING STIFFNESS MODEL

We record here the values of the eight constants of integration, $A_{1,2}$, $B_{1,2}$, $C_{1,2}$ and $D_{1,2}$ for the beam model with piecewise constant bending stiffness Eq. (3), and the four possible

combinations of clamped and simply supported end boundary conditions.

Equations (A1)–(A4) show the values of the constants where the beam is clamped at $x = 0$ and $x = 1$; Eq. (A5)–(A8) for clamped at $x = 0$ and simply supported at $x = 1$; Eq. (A9)–(A12) for simply supported at $x = 0$ and clamped at $x = 1$; and Eq. (A13)–(A16) for simply supported at $x = 0$ and $x = 1$.

$$A_1 = 0, \qquad A_2 = \frac{x_t^4}{24}(1-\Gamma)\frac{q}{EI_2}, \tag{A1}$$

$$B_1 = 0, \qquad B_2 = -\frac{x_t^3}{6}(1-\Gamma)\frac{q}{EI_2}, \tag{A2}$$

$$C_1 = \left[\frac{-3x_t^4 + 8x_t^3 - 6x_t^2}{24}(1-\Gamma) + \frac{1}{24}\right]\frac{q}{EI_2}, \qquad C_2 = \left[\frac{-3x_t^4 + 8x_t^3}{24}(1-\Gamma) + \frac{1}{24}\right]\frac{q}{EI_2}, \tag{A3}$$

$$D_1 = \left[\frac{x_t^4 - 2x_t^3 + 2x_t}{12}(1-\Gamma) - \frac{1}{12}\right]\frac{q}{EI_2}, \qquad D_2 = \left[\frac{x_t^4 - 2x_t^3}{12}(1-\Gamma) - \frac{1}{12}\right]\frac{q}{EI_2} \tag{A4}$$

$$A_1 = 0, \qquad A_2 = \frac{x_t^4}{24}(1-\Gamma)\frac{q}{EI_2}, \tag{A5}$$

$$B_1 = 0, \qquad B_2 = -\frac{x_t^3}{6}(1-\Gamma)\frac{q}{EI_2}, \tag{A6}$$

$$C_1 = \left[\frac{-x_t^4 + 4x_t^3 - 4x_t^2}{16}(1-\Gamma) + \frac{1}{16}\right]\frac{q}{EI_2}, \qquad C_2 = \left[\frac{-x_t^4 + 4x_t^3}{16}(1-\Gamma) + \frac{1}{16}\right]\frac{q}{EI_2}, \tag{A7}$$

$$D_1 = \left[\frac{x_t^4 - 4x_t^3 + 8x_t}{48}(1-\Gamma) - \frac{5}{48}\right]\frac{q}{EI_2}, \qquad D_2 = \left[\frac{x_t^4 - 4x_t^3}{48}(1-\Gamma) - \frac{5}{48}\right]\frac{q}{EI_2} \tag{A8}$$

$$A_1 = 0, \qquad A_2 = \frac{x_t^4}{24}(1-\Gamma)\frac{q}{EI_2}, \tag{A9}$$

$$B_1 = \left[\frac{-3x_t^4 + 8x_t^3 - 6x_t^2}{48}(1-\Gamma) + \frac{1}{48}\right]\frac{q}{EI_2}, \qquad B_2 = \left[\frac{-x_t^4 - 2x_t^2}{16}(1-\Gamma) + \frac{1}{48}\right]\frac{q}{EI_2}, \tag{A10}$$

$$C_1 = 0, \qquad C_2 = \frac{x_t^2}{4}(1-\Gamma)\frac{q}{EI_2}, \tag{A11}$$

$$D_1 = \left[\frac{x_t^4 - 6x_t^2 + 8x_t}{48}(1-\Gamma) - \frac{1}{16}\right]\frac{q}{EI_2}, \qquad D_2 = \left[\frac{x_t^4 - 6x_t^2}{48}(1-\Gamma) - \frac{1}{16}\right]\frac{q}{EI_2} \tag{A12}$$

$$A_1 = 0, \qquad A_2 = \frac{x_t^4}{24}(1-\Gamma)\frac{q}{EI_2}, \tag{A13}$$

$$B_1 = \left[\frac{-x_t^4 + 4x_t^3 - 4x_t^2}{24}(1-\Gamma) + \frac{1}{24}\right]\frac{q}{EI_2}, \qquad B_2 = \left[\frac{-x_t^4 - 4x_t^2}{24}(1-\Gamma) + \frac{1}{24}\right]\frac{q}{EI_2}, \tag{A14}$$

$$C_1 = 0, \qquad C_2 = \frac{x_t^2}{4}(1-\Gamma)\frac{q}{EI_2}, \tag{A15}$$

$$D_1 = \left[\frac{-x_t^2 + 2x_t}{12}(1-\Gamma) - \frac{1}{12}\right]\frac{q}{EI_2}, \qquad D_2 = \left[-\frac{x_t^2}{12}(1-\Gamma) - \frac{1}{12}\right]\frac{q}{EI_2} \tag{A16}$$

APPENDIX B. CONSTANTS OF INTEGRATION FOR THE RIGID ROD AND HINGE MODEL

We record here the values of the four constants of integration, A_2, B_2, C_2 and D_2 for the model described in section IV, where the arcuate zone is modelled by a rigid rod, the pectinate zone as a flexible beam of constant bending stiffness, with a hinge, or rotational spring, at $x = 0$, and the four possible combinations of clamped and simply supported boundary conditions.

Equations (B1)–(B4) show the values of the constants where the beam is clamped at $x = x_t$ and $x = 1$; Eq. (B5)–(B8) for clamped at $x = x_t$ and simply supported at $x = 1$; Eq. (B9)–(B12) for simply supported at $x = x_t$ and clamped at $x = 1$; and Eq. (B13)–(B16) for simply supported at $x = x_t$ and $x = 1$.

$$A_2 = \frac{((x_t-1)^3 + 48\kappa)x_t^2}{24(x_t-1)^3}\frac{q}{EI} \tag{B1}$$

$$B_2 = -\frac{x_t^5 - 2x_t^4 + 2(1+24\kappa)x_t^2 + (12\kappa-1)x_t + 12\kappa}{12(x_t-1)^3}\frac{q}{EI} \tag{B2}$$

$$C_2 = \frac{x_t^5 + x_t^4 - 8x_t^3 + 8(1+6\kappa)x_t^2 + (48\kappa-1)x_t - 1 + 48\kappa}{24(x_t-1)^3}\frac{q}{EI} \tag{B3}$$

$$D_2 = -\frac{x_t^4 - 2x_t^3 + 2(1+6\kappa)x_t - 1 + 12\kappa}{12(x_t-1)^3}\frac{q}{EI} \tag{B4}$$

$$A_2 = -\frac{x_t^6 - 6x_t^5 + 12x_t^4 + (-10 + 48\kappa)x_t^3 + (3 - 72\kappa)x_t^2}{48(x_t - 1)^3}\frac{q}{EI} \tag{B5}$$

$$B_2 = \frac{x_t^6 - 6x_t^5 + 6x_t^4 + (48\kappa + 8)x_t^3 + (-72\kappa - 15)x_t^2 + 6x_t - 48\kappa}{48(x_t - 1)^3}\frac{q}{EI} \tag{B6}$$

$$C_2 = \frac{3x_t^4 - 8x_t^3 + 6x_t^2 - 1 + 24\kappa}{16(x_t - 1)^3}\frac{q}{EI} \tag{B7}$$

$$D_2 = -\frac{3x_t^4 - 4x_t^3 - 6x_t^2 + 12x_t + 24\kappa - 5}{48(x_t - 1)^3}\frac{q}{EI} \tag{B8}$$

$$A_2 = \frac{3x_t^5 - 10x_t^4 + 12x_t^3 + (-6 + 72\kappa)x_t^2 + (1 - 48\kappa)x_t}{48(x_t - 1)^3}\frac{q}{EI} \tag{B9}$$

$$B_2 = -\frac{6x_t^5 - 15x_t^4 + 8x_t^3 + (6 + 144\kappa)x_t^2 + (-6 - 72\kappa)x_t + 1}{48(x_t - 1)^3}\frac{q}{EI} \tag{B10}$$

$$C_2 = \frac{x_t^5 - 6x_t^3 + (8 + 24\kappa)x_t^2 - 3x_t}{16(x_t - 1)^3}\frac{q}{EI} \tag{B11}$$

$$D_2 = -\frac{5x_t^4 - 12x_t^3 + 6x_t^2 + (24\kappa + 4)x_t - 3}{48(x_t - 1)^3}\frac{q}{EI} \tag{B12}$$

$$A_2 = -\frac{x_t(-1 + 4x_t - 4x_t^2 + 24\kappa + x_t^3)}{24(-1 + x_t)}\frac{q}{EI} \tag{B13}$$

$$B_2 = \frac{(x_t^4 - 4x_t^3 + (4 + 24\kappa)x_t - 1)}{24(-1 + x_t)}\frac{q}{EI} \tag{B14}$$

$$C_2 = \frac{x_t}{4}\frac{q}{EI} \tag{B15}$$

$$D_2 = -\frac{x_t + 1}{12}\frac{q}{EI} \tag{B16}$$

REFERENCES

P. Allaire, S. Raynor, and M. Billone (**1974**). "Cochlear partition stiffness — composite beam model", J. Acoust. Soc. Am. **55**(6), 1252–1258.

G. Barker (**2000**). *Pressure-feedforward and piezoelectric amplification models for the cochlea*, Ph.D. thesis, Department of Mechanical Engineering, Stanford University.

D. Brass (**2000**). "A macro-mechanical model of the guinea pig cochlea with realistic para-

meters", J. Acoust. Soc. Am. **107**(2), 894–907.

L. M. Cabezudo (**1978**). "The ultrastructure of the basilar membrane in the cat", Acta Otolaryngol (Stokh) **86**(3-4), 160–175.

N. P. Cooper (**1999**). "Radial variation in the vibrations of the cochlear partition", in: *Recent Developments in Auditory Mechanics*, edited by H. Wada, T. Takasaka, K. Ikeda, K. Ohyama, and T. Koike (World Scientific, Singapore), pp. 109–115.

N. P. Cooper (**2000**). "Radial variation in the sound-evoked vibrations of the cochlear partition", Assoc. Res. Otolaryngol **22**, 72. Abstract 254.

N. P. Cooper, and W. S. Rhode (**1992**). "Basilar membrane mechanics in the hook region of cat and guinea-pig cochleae: sharp tuning and nonlinearity in the absence of baseline position shifts", Hear. Res. **63**(1-2), 163–190.

P. Dallos, A. N. Popper, and R. R. Fay (**1996**). *The cochlea* (Springer).

R. M. Edge, B. N. Evans, M. Pearce, C. P. Richter, X. Hu, and P. Dallos (**1998**). "Morphology of the unfixed cochlea", Hear. Res. **124**(1-2), 1–16.

A. Fridberger, J. B. de Monvel, and M. Ulfendahl (**2002**). "Internal shearing within the hearing organ evoked by basilar membrane motion", J. Neurosci. **22**(22), 9850–9857.

J. M. Gere, and S. P. Timoshenko (**1991**). *Mechanics of materials* (Chapman & Hall, London).

R. Hallworth (**1995**). "Passive compliance and active force generation in the guinea pig outer hair cell", J. Neurophysiol. **74**(6), 2319–2328.

S. Iurato (**1962**). "Functional implications of the nature and submicroscopic structure of the tectorial and basilar membranes", J. Acoust. Soc. Am. **34**(9), 1386–1395.

K. D. Karavitaki, D. C. Mountain, and A. R. Cody (**1998**). "Electrically evoked micromechanical movements from the apical turn of the gerbil cochlea", in: *Diversity in Auditory Mechanics*, edited by E. R. Lewis (World Scientific, Singapore), pp. 392–398.

K.-M. Lim (**2000**). *Physical and mathematical cochlear models*, Ph.D. thesis, Department of Mechanical Engineering, Stanford University.

C. E. Miller (**1985**). "Structural implications of basilar membrane compliance measurements", J. Acoust. Soc. Am. **77**(4), 1465–1474.

K. E. Nilsen, and I. Russell (**1999**). "Timing of cochlear feedback: spatial and temporal representation of a tone across the basilar membrane", Nature Neuroscience **2**(7), 642–648.

K. E. Nilsen, and I. J. Russell (**2000**). "The spatial and temporal representation of a tone on the guinea-pig basilar membrane", Proc. Natl. Acad. Sci. **97**(22), 11751–11758.

E. S. Olson, and D. C. Mountain (**1994**). "Mapping the cochlear partition's stiffness to its cellular architecture", J. Acoust. Soc. Am. **95**(1), 395–400.

W. S. Rhode, and A. Recio (**2000**). "Study of mechanical motions in the basal region of the chinchilla cochlea", J. Acoust. Soc. Am. **107**(6), 3317–3332.

C. Richter, and P. Dallos (**1999**). "Vibrations of the inner hair cell stereocilia relative to the tectorial membrane and the reticular lamina", Assoc. Res. Otolaryngol. **21**, 211. Abstract 844.

Waterloo Maple Software (**1996**). *Maple V Programming Guide* (Springer-Verlag, New York).

C. R. Steele (**1974**). "Behavior of the basilar membrane with pure-tone excitation", J. Acoust. Soc. Am. **55**(1), 148–162.

J. A. Tolomeo, and M. C. Holley (**1997**). "Mechanics of microtubule bundles in pillar cells from the inner ear", Biophys. J. **73**(4), 2241–2247.

J. P. Wilson, and E. F. Evans (**1983**). "Some observations on the "passive" mechanics of cat basilar membrane", in: *Mechanisms of Hearing*, edited by W. R. Webster, and L. M. Aitkin (Monash University Press, Clayton), pp. 30–35.

TABLE I: Constants of integration for simple beam model

boundary condition		constants			
$x = 0$	$x = 1$	A	B	C	D
clamped	clamped	0	0	$\frac{1}{24}\frac{q}{EI}$	$-\frac{1}{12}\frac{q}{EI}$
clamped	simply supported	0	0	$\frac{1}{16}\frac{q}{EI}$	$-\frac{5}{48}\frac{q}{EI}$
simply supported	clamped	0	$\frac{1}{48}\frac{q}{EI}$	0	$-\frac{1}{16}\frac{q}{EI}$
simply supported	simply supported	0	$\frac{1}{24}\frac{q}{EI}$	0	$-\frac{1}{12}\frac{q}{EI}$

LIST OF FIGURES

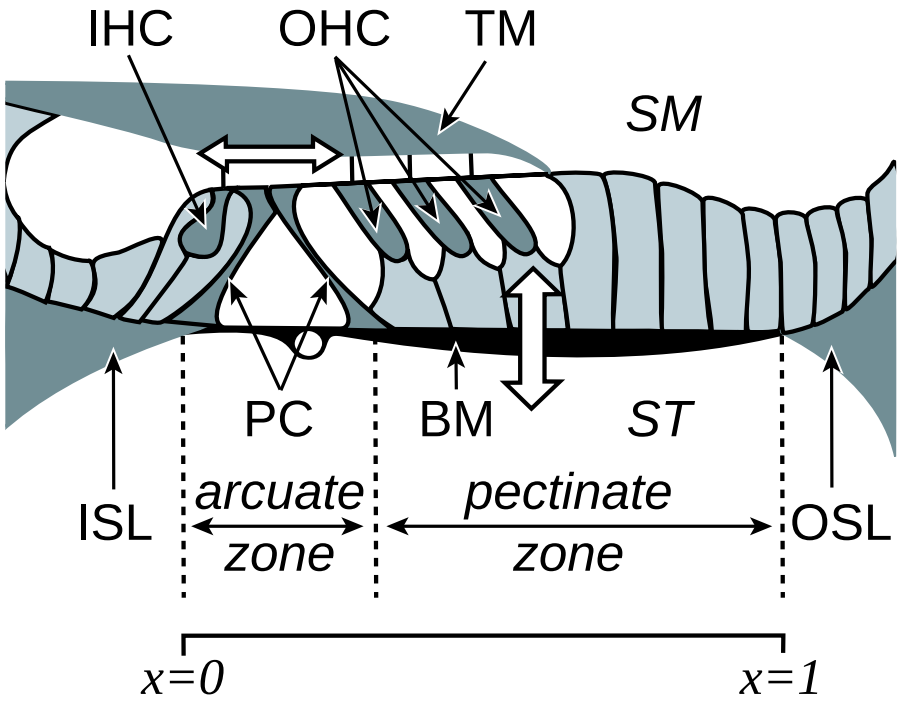

Figure 1: Schematic diagram of the mammalian cochlear partition. BM denotes the basilar membrane, whose endpoints attach to the inner spiral lamina (ISL) and outer spiral ligament (OSL). TM denotes tectorial membrane; PC denotes pillar cells; OHC and IHC outer and inner hair cells, respectively; SM and ST scala media and tympani, respectively.

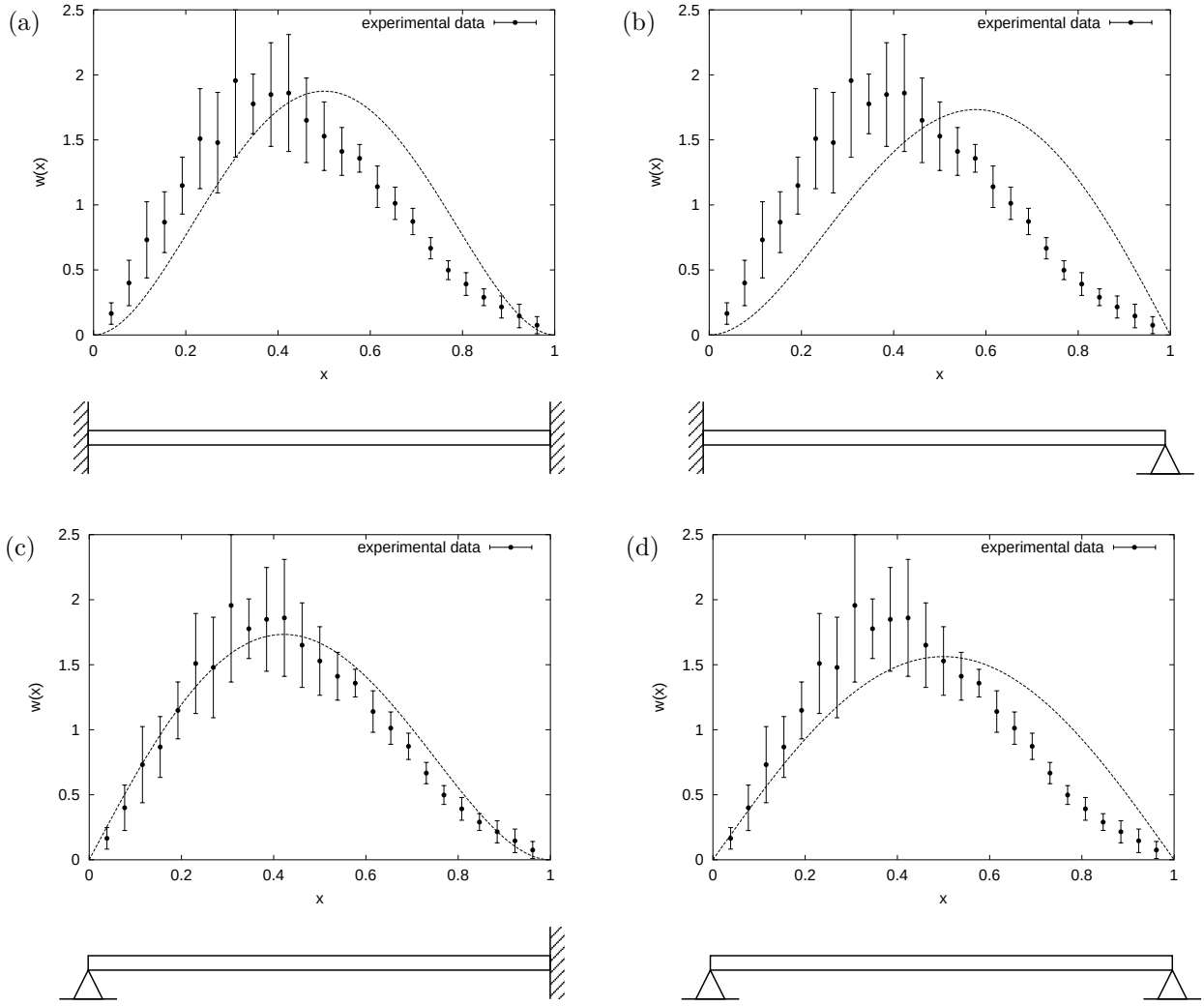

Figure 2: Graphs of membrane deflection versus radial position, for the constant bending stiffness beam model, with boundary conditions indicated by schematics below (▨ denotes clamped, △ simply supported).

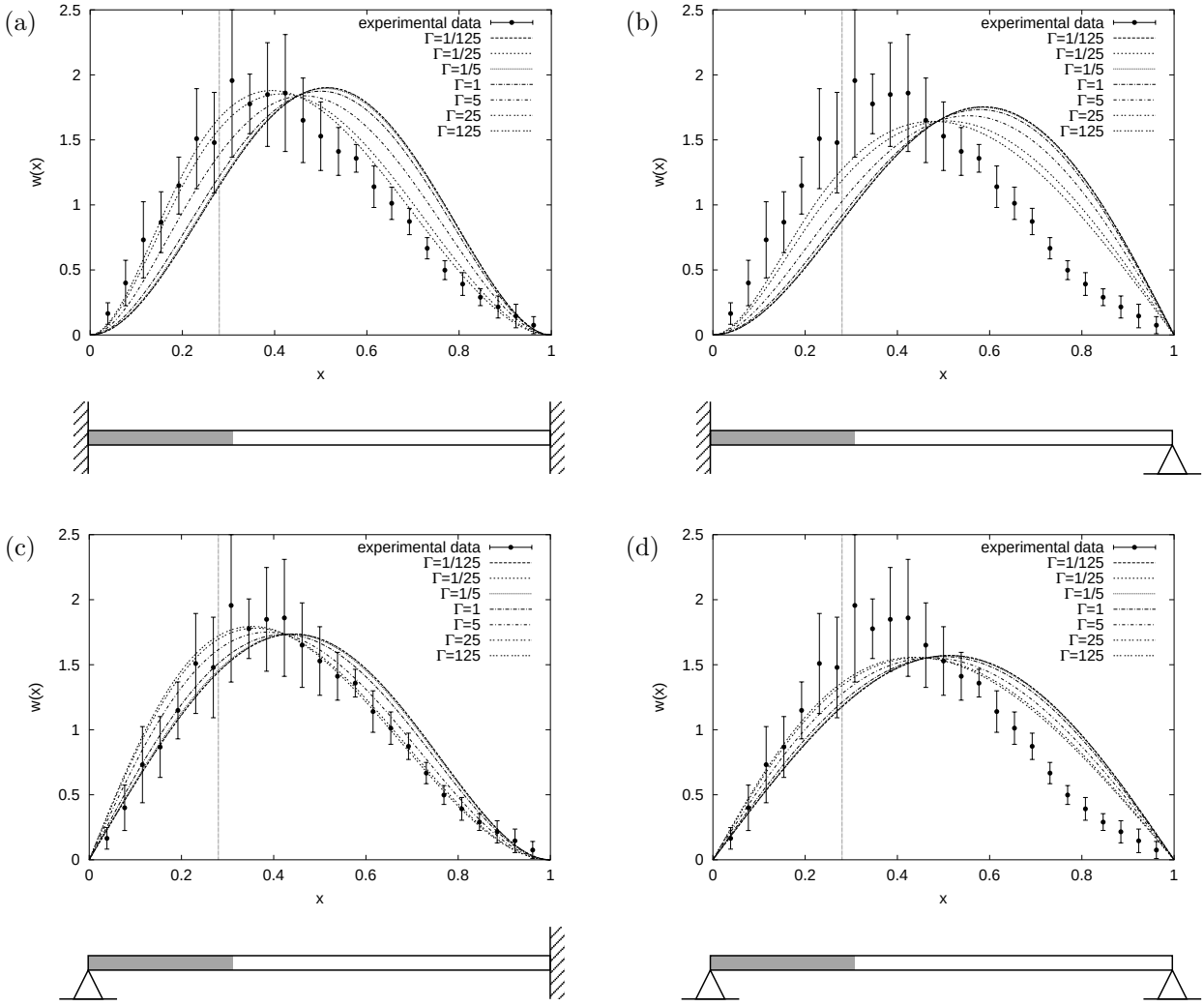

Figure 3: Piecewise constant bending stiffness beam model, for fixed $x_t = 0.28$ and varying bending stiffness ratio Γ, with boundary conditions indicated by schematics below (arcuate zone shaded).

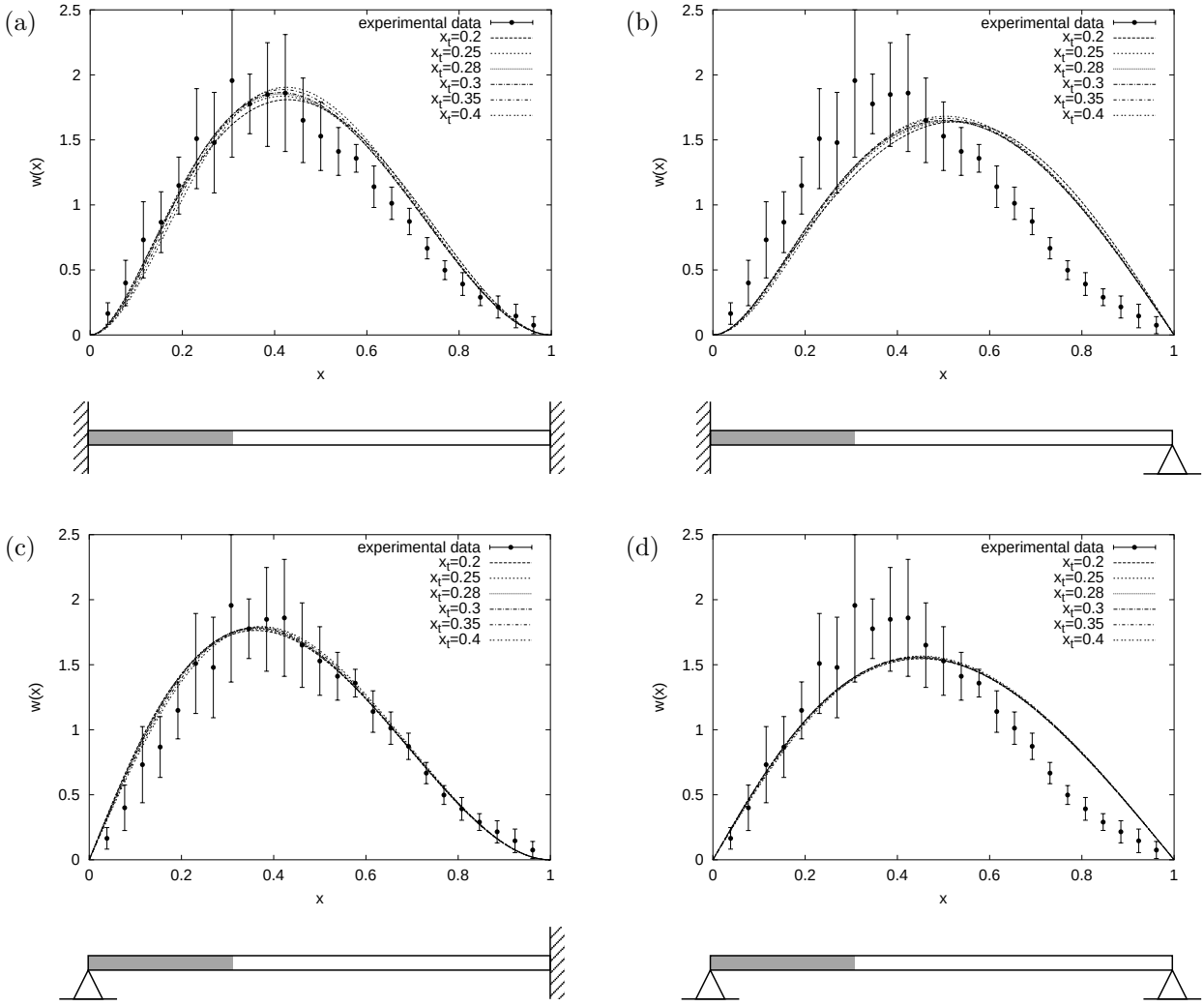

Figure 4: Piecewise constant bending stiffness beam model, for varying x_t and fixed stiffness ratio $\Gamma = 25$, with boundary conditions indicated by schematics below (arcuate zone shaded for a single x_t).

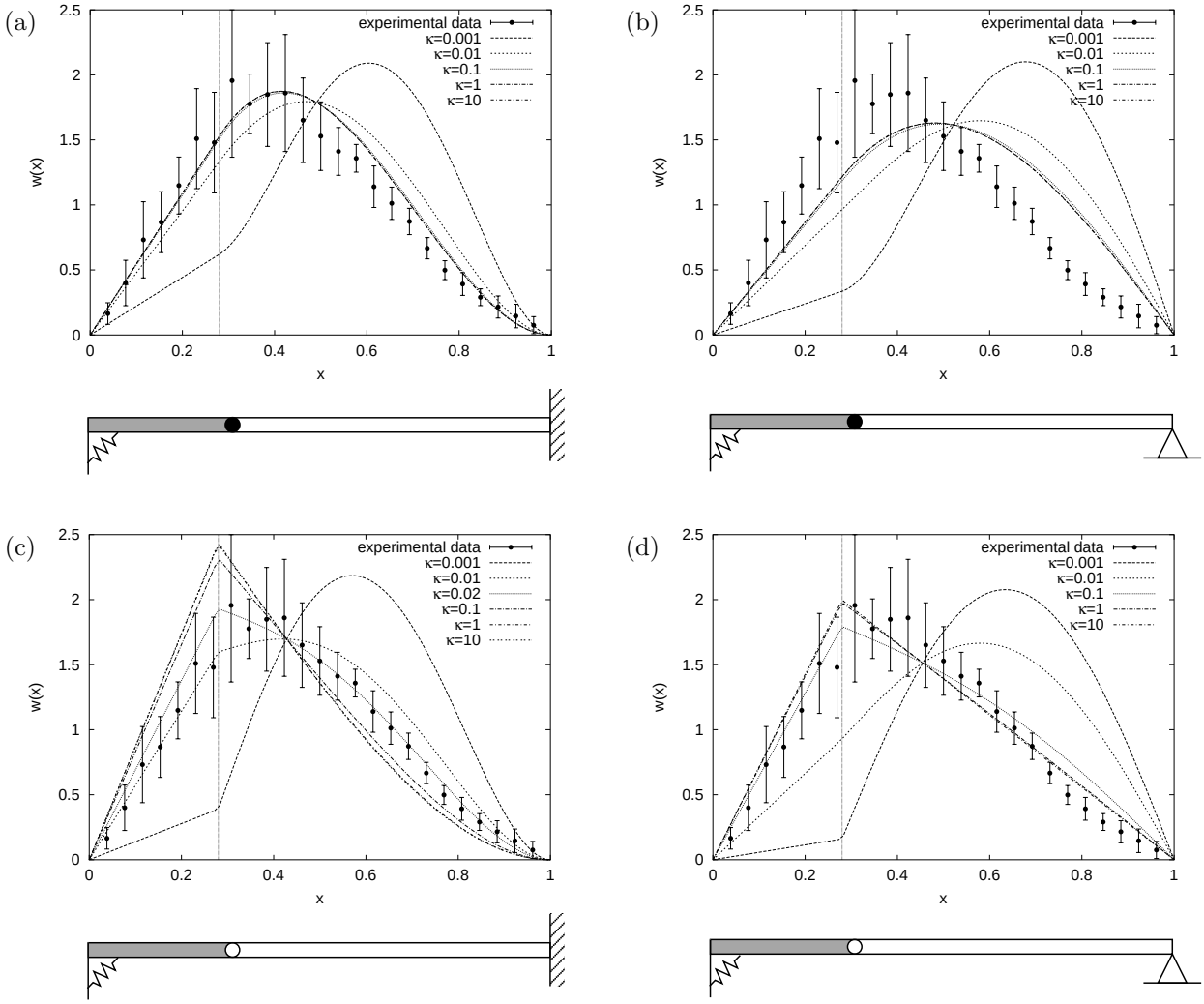

Figure 5: Rigid rod and hinge models, for varying hinge stiffness κ and fixed $x_t = 0.28$. Boundary conditions at $x = 1$ indicated by schematics below. Continuity conditions at $x = x_t$: (a) and (b) w and w' are continuous; (c) and (d) w and w'' are continuous.

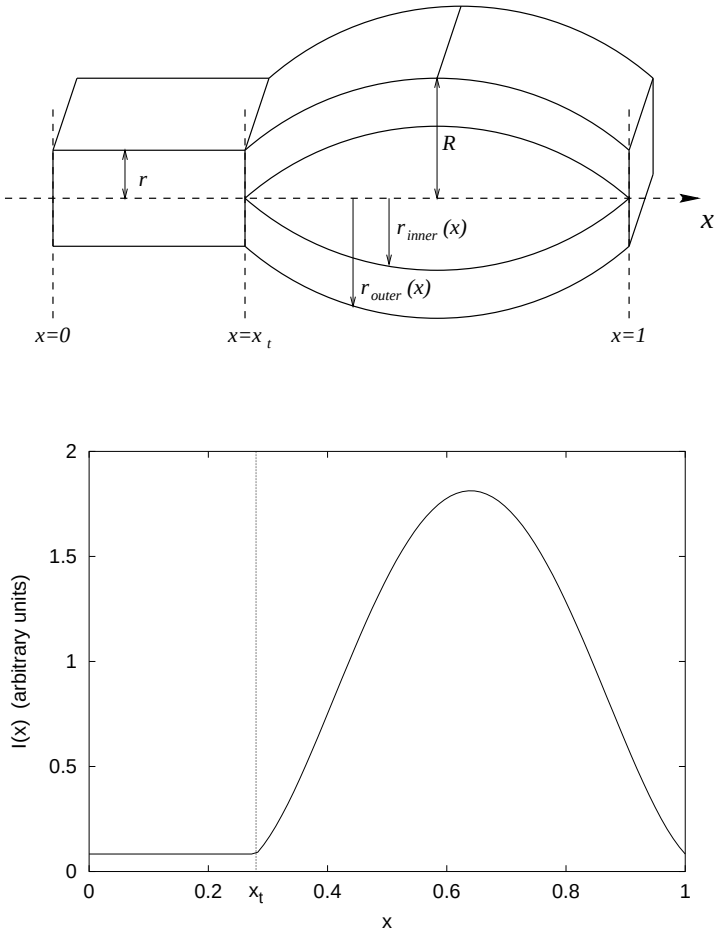

Figure 6: (above) Sketch profile of basilar membrane geometry, (below) plot of second moment of area for the variable thickness membrane with realistic parameter values

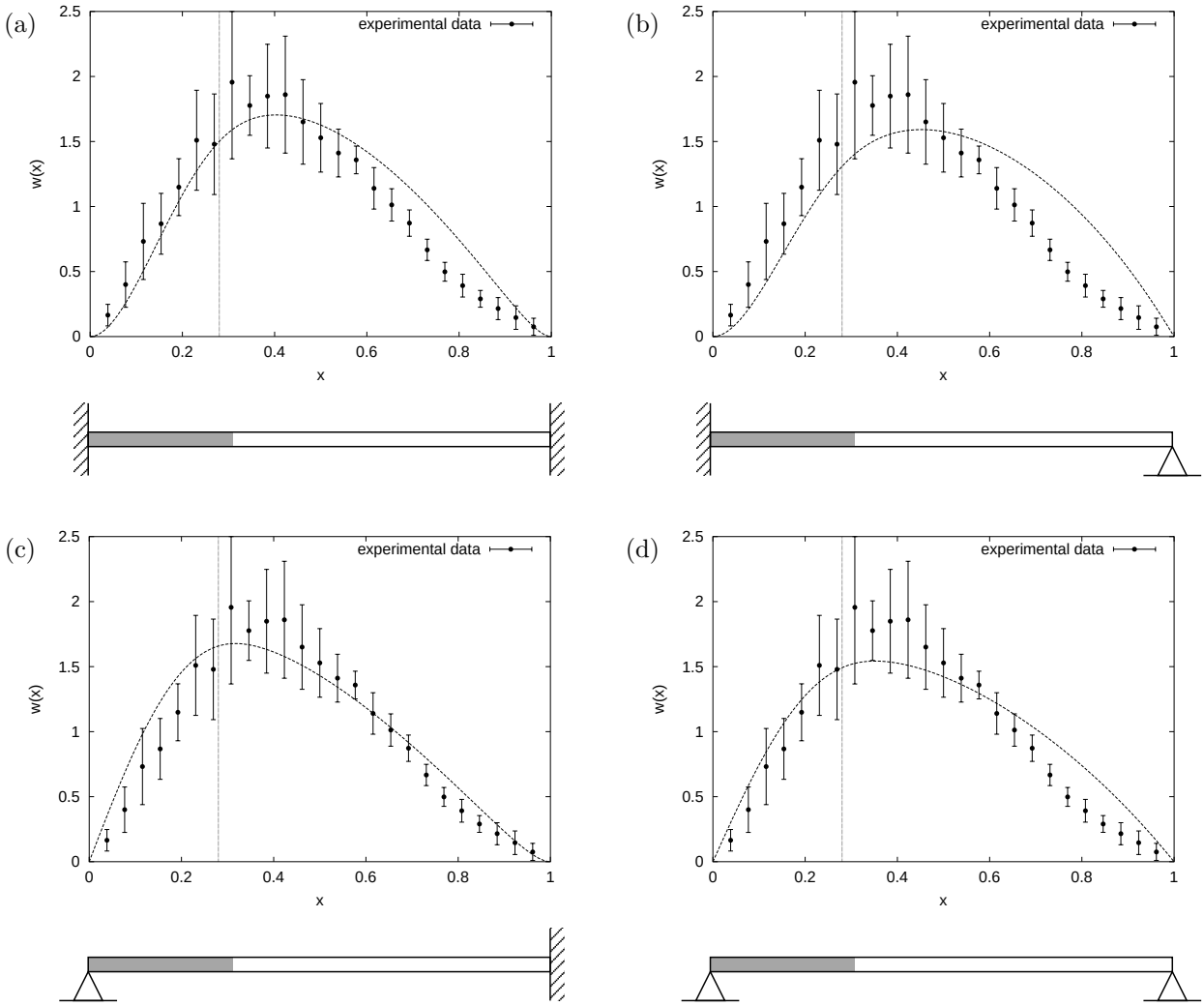

Figure 7: Continuously variable bending stiffness model for fixed $x_t = 0.28$, with boundary conditions indicated by schematics below.